ISSN 0021-3640, JETP Letters, 2026, Vol. 123, No. 2, pp. 85–92. © The Author(s), 2026. This article is an open access publication.
Russian Text © The Author(s), 2026, published in Pis'ma v Zhurnal Eksperimental'noi i Teoreticheskoi Fiziki, 2026, Vol. 123, No. 2, pp. 96–104.

OPTICS
AND LASER PHYSICS

Design Features of Optical Diffraction Neural Networks

A. V. Konovalova[a], A. A. Popkova[a], T. G. Baluian[a], and A. A. Fedyanin[a,*]

[a] *Faculty of Physics, Moscow State University, Moscow, 119991 Russia*

**e-mail: fedyanin@nanolab.phys.msu.ru*

Received October 18, 2025; revised November 25, 2025; accepted November 26, 2025

Recently, significant attention has been focused on finding and implementing approaches that would increase the efficiency of existing computational methods or create fundamentally new ones. One promising direction is the transition from digital to analog computing schemes, which allow for the design of high-performance specialized architectures based on known physical principles. In particular, a physical system in which a structure analogous to an artificial neural network can be implemented is a diffractive neural network. However, transferring computations to an analog platform entails the necessity of precise selection of a mathematical model that adequately accounts for the features of the physical implementation. In this work, the correctness of numerical modeling of a Fourier-diffractive neural network is experimentally tested, and the influence of the system configuration on the accuracy of the final computational result is numerically studied.

DOI: 10.1134/S0021364025609443

1. INTRODUCTION

The active development of neural networks (NNs) and machine learning methods creates broad opportunities for their application in various fields of science and technology [1–3]. In particular, machine learning opens up many promising research tasks in the field of photonics [4], including the design and optimization of optical elements and systems using machine learning [5–7]. Furthermore, photonic technologies enable the creation of optical accelerators for neural network computations [8, 9]. The need for the latter is driven by the increasing complexity of NN models and the growing demand for computational resources. Using classical computers for machine learning tasks is not an optimal solution, as the von Neumann architecture is characterized by a limited bandwidth bottleneck between the processor and memory [10].

To address these challenges, analog computing devices, particularly optical ones, are being explored [11]. They offer several advantages over electronic devices, such as low thermal losses, high speed and throughput, and ease of implementing parallel computations by utilizing various degrees of freedom inherent to light signals (wavelength, polarization, mode) [12]. Building optical NNs can not only accelerate computations and improve their energy efficiency but also enable the creation of neuromorphic architectures that, at the hardware level, reflect the distributed structure of NNs and fundamentally differ from the von Neumann paradigm [9, 13, 14].

One widespread configuration for free-space optical neuromorphic systems is the diffractive neural network (DNN) [15]. As an analog to convolutional neural networks, this architecture appears promising for the use in matrix computations and all-optical image processing [16, 17]. The layers of a DNN consist of amplitude and/or phase masks, whose parameters serve as synaptic weights determined during the computer-based training of the network model. This approach offers great flexibility, allowing for the design of task-specific systems with diverse architectures [18] and signal modulation methods [19, 20], multi-task networks [21], as well as active neural networks capable of training directly on the optical setup [22].

When training DNNs, it is necessary to account for the limited accuracy of mathematical models, as well as the correctness of their application in describing the physical phenomena occurring within the optical system. For instance, the discrete Fourier transform is often used to model light propagation in the system, which, on the one hand, significantly increases calculation speed, but also imposes specific constraints on the choice of parameters for the model system, related to the conditions of its use [23].

This paper focuses on diffractive neural networks operating in the Fourier domain (FDNN) [24]. This architecture incorporates the common optical approach of analog Fourier filtering into DNNs [25, 26]. An experimental study of the correctness of modeling the network elements is performed, along with a numerical analysis of the influence of various FDNN parameters on its operational accuracy.

2. STRUCTURE OF THE FDNN

Figure 1 shows a schematic of a typical FDNN using a network solving the task of classifying handwritten digits from 1 to 4 as an example. The input image in the system is formed by a plane light wave passing through an amplitude mask. The mask has a profile matching an element from the MNIST database [27] and is located in the front focal plane of a converging lens. The Fourier transform of the original image is formed in the back focal plane and is subsequently processed by a series of diffractive layers. The output image from the FDNN is formed by the second converging lens, which performs the inverse Fourier transform. In the output plane, each class corresponds to a specific area of the image (highlighted by red rectangles in Fig. 1). The goal of training the FDNN is to select the geometric parameters of the computational layers that ensure the focusing of radiation into the area corresponding to the class of the input image. The computational layers of the FDNN are phase masks, each consisting of an array of $N \times N$ pixels—regular rectangular cuboids of varying heights—which act as optical neurons. According to the Huygens–Fresnel principle, each point of a diffractive layer can be considered as a source of secondary waves, whose amplitude and phase are determined by the incident wave $U(x, y)$ and the complex transmission coefficient t of the layer at that point:

$$U'(x, y) = U(x, y)t(x, y). \quad (1)$$

Here, we consider only phase modulation, since the absorption coefficient of the mask material and its thickness are small, and it is assumed that absorption does not contribute significantly to signal modulation. Therefore, the transmission coefficient in the model takes the form $t(x, y) = e^{i\phi(x,y)}$, where $\phi(x, y)$ is the phase delay acquired by the radiation passing through the mask. The image obtained at the output of a network layer is formed as a result of the interference of secondary waves created by the diffractive layer. The delays introduced by each pixel determine the interference conditions and can be considered as synaptic weights [12, 15].

Thus, for comparison of the mathematical model operation with the real system, it is necessary to examine the following stages:

- light propagation within the FDNN optical system;
- light focusing using a converging lens;
- light propagation through a phase mask.

Furthermore, important issues are the limitations imposed on the mathematical model by existing manufacturing technologies and the accuracy of electronic components, in particular, the sensitivity of the detection system located in the output plane.

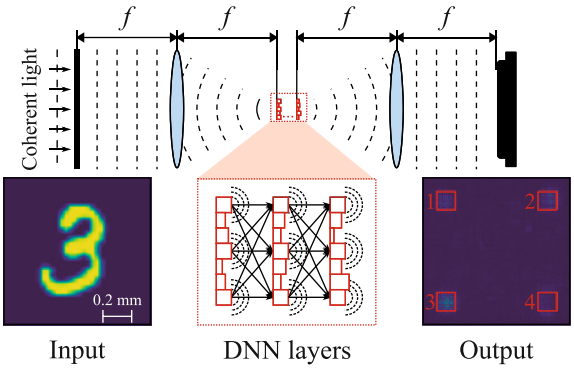

Fig. 1. (Color online) Schematic of an optical FDNN for a classification task.

3. CALCULATION OF RADIATION PROPAGATION IN SPACE

To calculate the field distribution during light propagation over a distance z we will use its angular spectrum (spatial Fourier transform) [25]:

$$A\left(\frac{\alpha}{\lambda}, \frac{\beta}{\lambda}, 0\right) = \iint_{-\infty}^{+\infty} U(x, y, 0) e^{-i2\pi\left(\frac{\alpha}{\lambda}x + \frac{\beta}{\lambda}y\right)} dxdy, \quad (2)$$

where $U(x, y, 0)$ is the spatial distribution of the electromagnetic field in the plane of the input image; λ is the radiation wavelength; α, β are the angles between the wave vector $\mathbf{k}$ and the Ox, Oy axes, respectively. The quantities $f_x = \frac{\alpha}{\lambda}$ and $f_y = \frac{\beta}{\lambda}$ are the spatial frequencies.

The angular spectra in planes separated by a distance z are related by the expression:

$$A\left(\frac{\alpha}{\lambda}, \frac{\beta}{\lambda}, z\right) = A\left(\frac{\alpha}{\lambda}, \frac{\beta}{\lambda}, 0\right) e^{i\frac{2\pi}{\lambda}\sqrt{1-\alpha^2-\beta^2}z}. \quad (3)$$

From this, the field distribution in plane z can be found as:

$$U(x, y, z) = \mathcal{F}\left(\mathcal{F}(U(x, y, 0)) e^{i\frac{2\pi}{\lambda}\sqrt{1-\alpha^2-\beta^2}z}\right), \quad (4)$$

where $\mathcal{F}$ denotes the Fourier transform. Numerical modeling of light propagation uses the Fast Fourier Transform (FFT) [28]. The use of FFT determines the choice of the computational grid step: if the step is too large, aliasing effects [23] may occur, distorting the obtained Fourier spectrum, while using too fine step significantly slows down the calculations. In this work, a step not exceeding several radiation wavelengths was chosen, allowing a compromise between computation speed and accuracy.

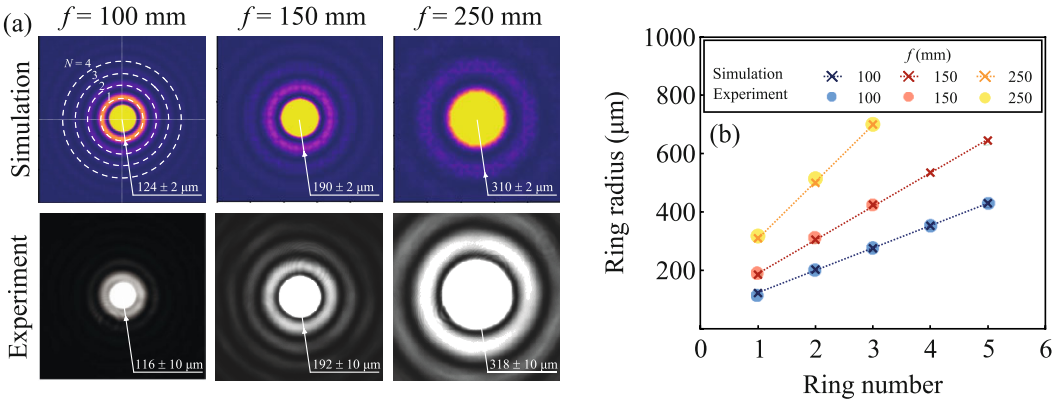

Fig. 2. (Color online) (a) Fourier transforms of a circular aperture with a radius of 900 μm, formed by lenses with different focal lengths: simulation (top row) and experiment (bottom row). (b) Comparison of simulated (×) and experimental (○) dependences of the ring radius in the Fourier transform of the aperture on the ring number.

4. MODELING LIGHT FOCUSING WITH A CONVERGING LENS

Converging lenses are used for direct and inverse Fourier transforms in the optical neural network. To obtain the field $U'(x, y)$ directly after the lens, it is necessary to multiply the field distribution in front of the lens $U(x, y)$ by the introduced phase delay [25]:

$$U'(x, y) = U(x, y)\exp\left[-i\frac{\pi}{\lambda f}(x^2 + y^2)\right]. \quad (5)$$

The approximation used does not account for the finite size of the lens aperture and the associated vignetting effect—the darkening of the image away from the optical axis—which does not affect accuracy due to the finite size of the detection area.

To verify the modeling of light propagation in space and the transformation performed by the lens, Fourier transforms of a circular aperture were obtained numerically and experimentally using lenses with different focal lengths (100, 150, and 250 mm). For this purpose, an experimental setup was assembled consisting of a radiation source (a diode laser with a wavelength of 676 nm), a beam-expanding lens system to provide parallel illumination, an aperture with a diameter of 900 μm, a converging lens, and a camera. The aperture was placed in the front focal plane of the lens; a camera visualizing the resulting intensity distribution was placed in the back focal plane. In the numerical simulation, a plane wave was incident on the aperture. The aperture model was implemented as follows: radiation passing through the aperture retained its amplitude and phase; radiation incident on the opaque part of the aperture was completely absorbed. The propagation of radiation from the aperture plane to the lens and from the lens to the back focal plane was calculated using formula (4), and the phase delay introduced by the lens was calculated using formula (5).

The Fourier transform of a circular aperture is a series of rings, whose size depends on the radius of the original circle and the focal length of the lens forming the transform (Fig. 2a). To compare the images obtained from calculations and experiments, dependences of the ring radii on their number, counting from the center, were plotted (Fig. 2b). The graph shows good agreement between the Fourier transforms obtained using lenses with the same focal lengths. This allows us to conclude that this method is correct for calculating the propagation of an optical signal through a lens in the computer model of the FDNN.

5. MODELING LIGHT PROPAGATION THROUGH A PHASE MASK

During the training of the neural network computer model, a matrix of phase delays introduced by the neurons of the diffractive layer is determined. For a known refractive index of the mask material n_{res} at a given wavelength λ the phase delays ϕ_i are related to the pixel heights d_i as follows:

$$d_i = \phi_i \frac{\lambda}{2\pi(n_{res} - n_{air})}, \quad (6)$$

where n_{air} is the refractive index of the mask surrounding medium. The typical heights of mask pixels with a refractive index $n_{res} = 1.65$ are less than 1 μm. A method providing the necessary height resolution is two-photon laser lithography, which has proven effective for fabricating photonic devices [29], including an optical linear perceptron [30]. The main advantage of this technique for DNN applications is the capability for rapid prototyping of samples with sufficient spatial resolution for the visible spectral range, which is particularly promising for designing passive circuits to solve specific tasks.

To verify the results of calculating light propagation through a phase mask, a simple system consisting of

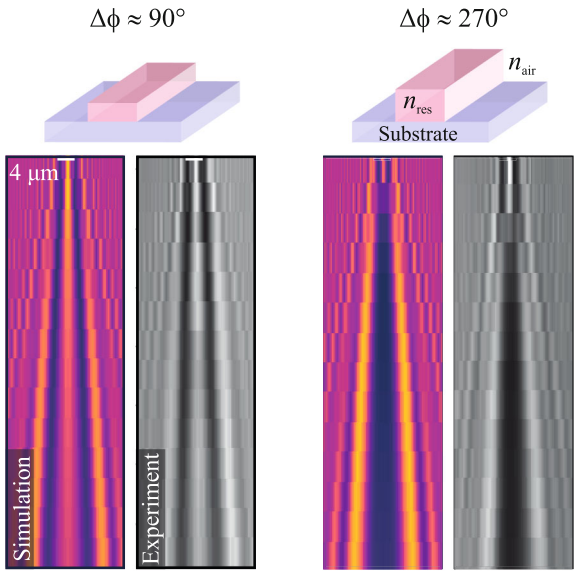

Fig. 3. (Color online) Light diffraction patterns from phase slits introducing phase shifts of 90° (left) and 270° (right). For each slit, the results of numerical simulation (color image—online) are shown on the left, and the experimental results are on the right.

single-phase slits—strips of material introducing a constant phase shift—of various thicknesses was chosen. The experimental sample was fabricated on a cover glass substrate using two-photon laser lithography [31] and consisted of a series of strips 4 μm wide, with thicknesses varying from 0 to 1.2 μm in steps of 0.1 μm; the strip length was about 50 μm, allowing the system to be considered as one-dimensional one.

Figure 3 shows the radiation propagation pattern when passing through phase slits introducing phase shifts approximately equal to 90° and 270°. The images represent a set of cross-sections of the intensity distribution at different distances from the studied object. The experimentally obtained cross-sections were extracted from a series of images taken while moving the sample along the optical axis of the system. This varied the distance between the phase slit and the objective, allowing the construction of the field distribution on the camera matrix in a plane at a fixed distance from the slit. In the numerical simulation, it was assumed that the field immediately in front of the sample is a plane wave, which acquires a constant phase delay upon passing through the slit; radiation passing outside the slit remains unchanged. The field at the selected distance from the sample was calculated using formula (4). From the resulting images, similar to the experiment, cross-sections were extracted and light propagation patterns were formed.

The presented images show that the experimental results correspond to the numerical modeling. It can also be observed that when the phase shift changes, the intensity maximum in the center of the pattern is replaced by a minimum, which allows changing the radiation distribution pattern near the next neural network layer by proper modulation of the thickness of an individual pixel. This mechanism of the influence of the phase delay introduced by a pixel on the intensity of light incident on the pixels of the next layer underlies the role of pixel thickness as the synaptic weight of an optical neuron.

6. PIXEL SIZE OF THE PHASE MASK

The distribution of electromagnetic field intensity behind the mask is influenced not only by the thicknesses of the pixels but also by their lateral dimensions. Changing the width of a phase slit alters the angles characterizing the interference maxima and minima, which can be used to modify the overall network connectivity [32]. However, from the perspective of designing a complete system, the geometric parameters of phase masks, specifically the size and number of pixels, are significantly constrained by the fabrication method. The ratio between the size of the image incident on the diffractive layer and the pixel size will affect the network efficiency. This is because a different number of optical neurons will participate in processing a given portion of the image. In an FDNN, the Fourier transform of the input image is send to the first computational layer, and its size can be adapted for given phase mask parameters by selecting the focal length of the lens performing the Fourier transform. To study the influence of the Fourier transform size on the DNN performance, a model of a two-layer network trained to classify digits from 1 to 4 was chosen. Phase masks with pixel sizes of 4 and 10 μm and lateral dimensions of 20 and 8 pixels, respectively, were selected, allowing the overall system dimensions to be maintained. Typical scales of the Fourier transforms and masks in the studied system are shown in Fig. 4a.

Figure 4b shows the training results for networks using lenses with different focal lengths (the input image size is fixed). It can be seen that as the focal length decreases, and consequently the size of the Fourier transform decreases, the classification accuracy increases. This can be explained by the fact that more spatial harmonics fall on the phase mask, thereby providing the DNN with more information about the original image. However, with further reduction in focal length, accuracy begins to decline, as the resolution of the phase mask becomes insufficient to account for finer details of the Fourier spectrum, which become smaller than the mask pixels. This is supported by the fact that with a higher pixel density in the mask, the accuracy maximum shifts towards a smaller focal length, corresponding to a smaller Fourier transform size.

This approach to accounting for the pixel size of computational layers during the optical system design phase can also be applied to DNNs operating in real space. This will allow for the selection of parameters

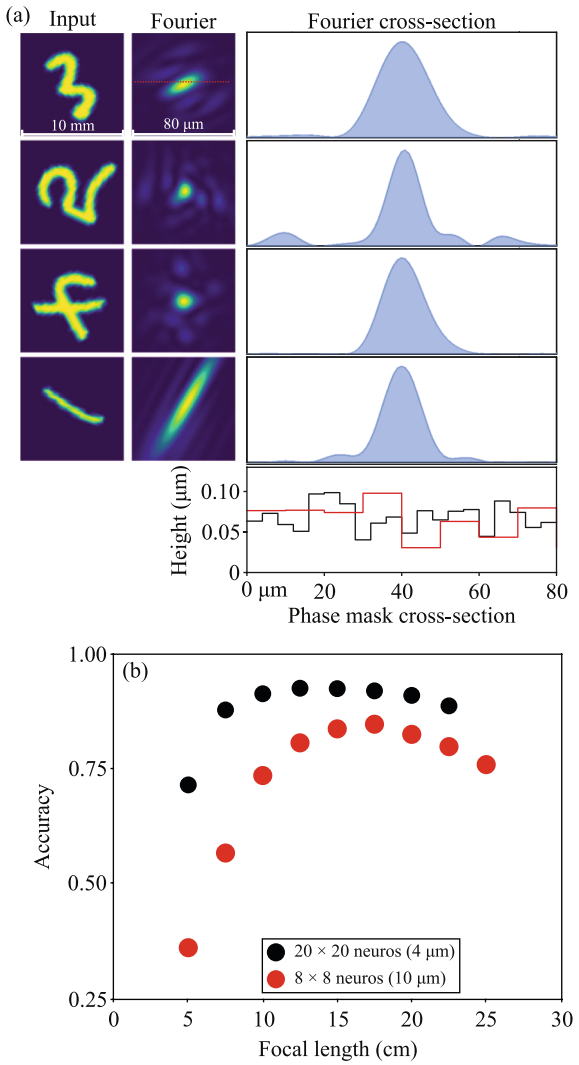

Fig. 4. (Color online) (a) Comparison of the sizes of Fourier transforms of different digits ($f = 20$ cm) and the phase mask profile. (b) Dependence of classification accuracy on the lens focal length. The pixel size of the phase mask with 20 × 20 neurons is 4 μm (black curve), with 8 × 8 neurons—10 μm (red curve).

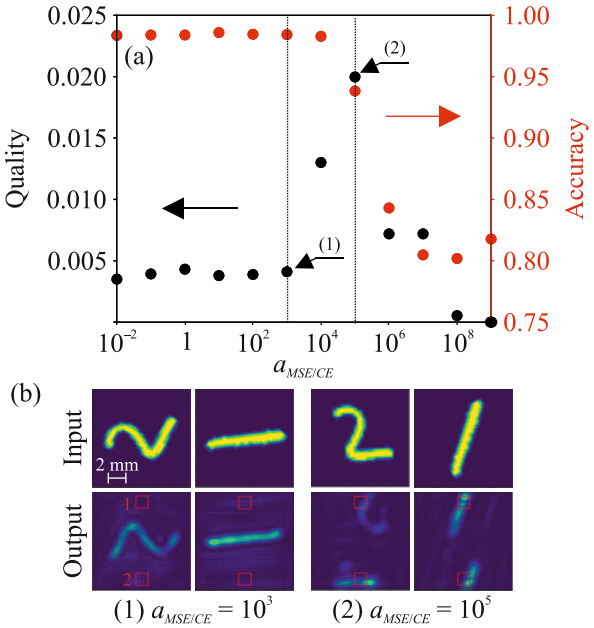

Fig. 5. (Color online) (a) Dependence of the Quality parameter and classification accuracy on the choice of the loss function. (b) Example of the network operation for different values of the ratio between the mean squared error and cross-entropy in the loss function, corresponding to the dashed lines (1) and (2) in panel (a).

for lens systems or objectives used to form the image in the plane of the input layer, based on the characteristics of the images in the tasks being solved.

7. ACCOUNTING FOR DETECTOR SENSITIVITY

An important parameter of a neural network that determines the training outcome is the loss function L. If cross-entropy [2] is used to train the network, the radiation intensity incident on the detectors differs little from the background illumination intensity, making measurements difficult. When using the mean squared error as the loss function, radiation is focused into the target detector areas, but classification accuracy decreases. To leverage the advantages of both functions, we introduce their linear combination:

$$L = \alpha_{MSE/CE} L_{MSE} + L_{CE}, \tag{7}$$

where L_{MSE} is the mean squared error, L_{CE} is the cross-entropy, $\alpha_{MSE/CE}$ is a scaling coefficient.

To choose the optimal balance between the two functions, we introduce a dimensionless quantity Quality, which accounts for both prediction accuracy and the contrast between intensities in the target and non-target areas of the detector. We define this parameter as:

$$\text{Quality} = \frac{T_l - F_l}{\max(T_l - F_l)} \cdot \frac{A - \min(A)}{\max(A) - \min(A)}, \tag{8}$$

where A is the classification accuracy, T_l is the total radiation intensity incident on the target detector, F_l is the average total intensity on the non-target detectors; the maximum and minimum values of the quantities are chosen from the values obtained on the test fragment of the database.

The form of the Quality function was studied using the example of a single-layer network for binary classification. While such a system cannot solve more complex tasks with acceptable accuracy, it provides a clear way to track the influence of the loss function on the intensity distribution pattern in the system output plane. The dependence of the Quality parameter on the coefficient $\alpha_{MSE/CE}$ is shown in Fig. 5a. It has a

maximum at $\alpha_{MSE/CE} = 10^5$, where the classification accuracy begins to decline, amounting to 95%, while maintaining good light localization in the detectors. Figure 5b shows characteristic patterns of intensity distribution in the detector plane, corresponding to a dominant contribution from cross-entropy ($\alpha_{MSE/CE} \le 10^3$) on the left and an increased role of mean squared error ($\alpha_{MSE/CE} \ge 10^5$) on the right. The images show the aforementioned features of FDNNs trained using one of the two considered loss functions.

8. ACCOUNTING FOR HEIGHT DISCRETIZATION

When training a DNN model, the phase delays introduced by the computational layers can vary continuously. However, any fabricating process implies finite precision: the minimum step for changing the pixel heights of the phase masks (the discretization step) will be limited.

To assess the influence of the limited fabricating precision of computational layers on the network performance, several phase masks providing different accuracy levels for a binary classification task in a single-layer network were selected. These masks were used to validate the network model for various discretization steps: the phase delay values introduced by the pixels of the diffractive layer were rounded to the nearest discrete values for the chosen step (Fig. 6a). Then, the classification accuracy with the obtained mask was evaluated on a validation set (Fig. 6b). It is evident that across a wide range of phase discretization step values (from 0 to $\pi/2$) the accuracy changes slightly. With further increase in the discretization step, binary classification accuracy drops sharply to 0.5, which corresponds to random guessing. The observed behavior can be interpreted using the results of modeling light diffraction on a single pixel. The magnitude of the introduced phase delay influences the field distribution behind the pixel, with the signal maximum in the center of the pattern switching to a minimum at a phase delay value of around π. Thus, as the discretization step increases, the proportion of pixels for which rounding changes the characteristic field distribution behind them also increases. However, for a step not exceeding $\pi/2$, the proportion of such pixels is small, which provides some freedom in choosing the manufacturing method due to the limited requirements for its resolution.

For masks discretized in phase delays with a step size x, the network classification accuracy (A_{est}) can be estimated as:

$$A_{\text{est}} = A_{\max} - \left(A_{\max} - \frac{1}{2}\right)\left(\frac{e^{2x} - 1}{e^{2\pi} - 1}\right). \qquad (9)$$

This approximation was chosen based on the following considerations: maximum accuracy $A_{\max}$ is observed

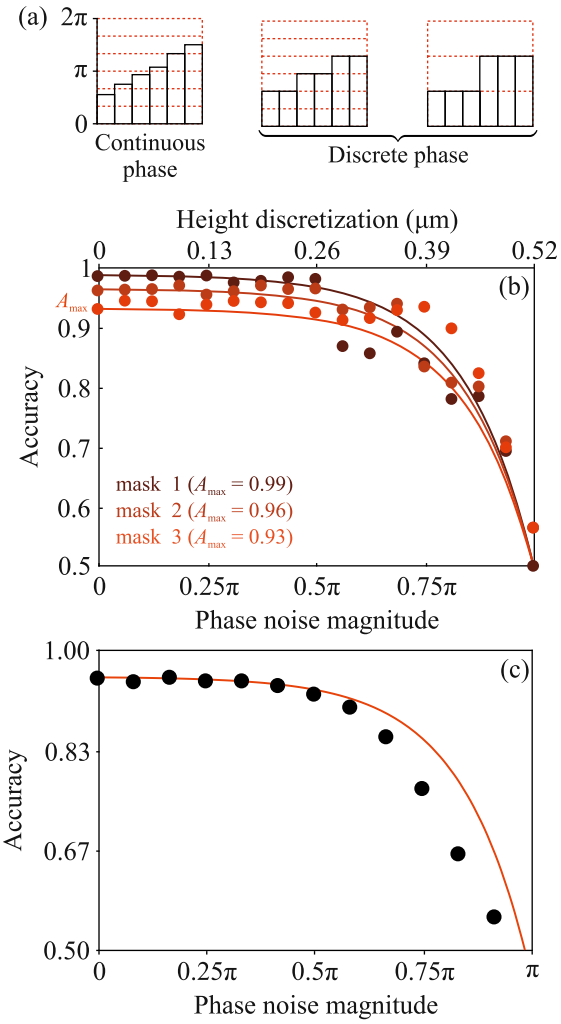

Fig. 6. (Color online) (a) Schematic illustration of the discretization concept. (b) Dependence of classification accuracy on the discretization step of phase mask pixels in height and phase for various masks. (c) Dependence of classification accuracy on the amplitude of phase noise. Dots show the results of numerical simulation, curves show approximations according to formula (9).

in the absence of discretization; the minimum value for binary classification is 0.5, corresponding to random guessing, and is reached in the obtained dependences for a discretization step of about π. Thus, points $(A_{\max}, 0)$ and $(0.5, \pi)$, can be considered as known onces, and the decay pattern is well described by an exponential dependence. In Fig. 6b, the estimates for various masks are indicated by solid curves. The graph shows that the proposed approximation aligns with the numerical modeling. This method of estimating accuracy drop is useful when selecting experimental parameters is based on the resolution of the manufacturing method.

Distortion of pixel heights in phase mask systems can arise not only from the limited precision of the

manufacturing method but also due to the influence of random processes. To test the resilience of FDNNs to such effects, let's examine the change in classification task accuracy when varying an individual pixel's height by a random amount. Then, the phase delay ϕ_i, introduced by a pixel can be expressed as:

$$\phi_i = \phi_i^{\text{model}} + \Delta\phi_i, \quad (10)$$

where ϕ_i^{model} is the phase delay value obtained during the computer model training; $\Delta\phi_i$ is the phase noise. For phase noise whose magnitude is uniformly distributed on the interval $[-\Delta\phi^{\max}, +\Delta\phi^{\max}]$, the dependence of classification accuracy on the amplitude $\Delta\phi^{\max}$ has the form presented in Fig. 6c. The influence of random phase noise on classification accuracy is similar to the effect of pixel height discretization: for phase deviations within $\pi/2$ accuracy decreases insignificantly; in the interval from $\pi/2$ to π a sharp drop is observed. The quantitative parameters of this drop, however, depend significantly on the type of noise distribution, highlighting the importance of considering the specifics of the arising errors when designing real devices. The obtained results allow us to conclude that to preserve the network functionality at a level close to the theoretical maximum, the manufacturing of phase masks must ensure the accuracy of forming the phase delay on an individual pixel to be on the order of $\pi/4$.

9. CONCLUSIONS

We have experimentally verified the calculations of light propagation through the elements of a Fourier-diffractive neural network, thereby demonstrating the correctness of the applied approximations and the applicability of the described mathematical model. For a single optical neuron—a pixel of the diffractive layer—the physical basis of the analogy between the synaptic weight of a neuron and the phase delay introduced by the pixel was illustrated.

The analysis conducted in this work on the influence of the FDNN configuration on the classification accuracy enables the consideration of various optical system parameters impact on network efficiency during the design phase. A promising direction for the further research can be the investigation of the dependence of DNN connectivity on the geometric parameters of the system of diffractive layers and the wavelength of the radiation used. Such an assessment can be useful both from the perspective of designing networks with a predetermined connectivity and for saving computational resources during training.

Furthermore, the work attempted to assess the influence on network performance of factors typical for a real optical system. In particular, we demonstrated a decrease in classification accuracy in a network with discretely varying phase mask pixel heights and provided a simple method for estimating accuracy for a chosen discretization step. The influence of the loss function choice on the pattern of radiation intensity distribution in the detector plane was shown. The presented analysis does not exhaust all factors associated with transitioning from simulation to experiment. Specifically, for the case of multi-layer DNNs, possible inaccuracies related to the positioning of diffractive layers should be considered. The implementation in FDNNs of training algorithms that increase the system robustness to lateral shifts [33] and the investigation of their influence on network efficiency can constitute the next step in this topic.

ACKNOWLEDGMENTS

The authors thank K.R. Safronov for assistance in developing the software for FDNN simulation.

FUNDING

This work was supported by the Russian Science Foundation, project no. 25-12-00355, and by the Noncommercial Foundation for the Development of Science and Education "Intellect."

CONFLICT OF INTEREST

The authors of this work declare that they have no conflicts of interest.

OPEN ACCESS

This article is licensed under a Creative Commons Attribution 4.0 International License, which permits use, sharing, adaptation, distribution and reproduction in any medium or format, as long as you give appropriate credit to the original author(s) and the source, provide a link to the Creative Commons license, and indicate if changes were made. The images or other third party material in this article are included in the article's Creative Commons license, unless indicated otherwise in a credit line to the material. If material is not included in the article's Creative Commons license and your intended use is not permitted by statutory regulation or exceeds the permitted use, you will need to obtain permission directly from the copyright holder. To view a copy of this license, visit http://creativecommons.org/licenses/by/4.0/

REFERENCES

1. C. M. Bishop, "Neural networks and their applications," Rev. Sci. Instrum. **65**, 1803 (1994).
2. I. Goodfellow, Y. Bengio, and A. Courville, *Deep Learning* (MIT Press, Cambridge, 2016).
3. O. I. Abiodun, A. Jantan, A. E. Omolara, K. V. Dada, N. A. E. Mohamed, and H. Arshad, "State-of-the-art in artificial neural network applications: A survey," Heliyon **4**, e00938 (2018).
4. G. Genty, L. Salmela, J. M. Dudley, D. Brunner, A. Kokhanovskiy, S. Kobtsev, and S. K. Turitsyn,

"Machine learning and applications in ultrafast photonics," Nat. Photon. **15**, 91 (2021).

5. K. R. Safronov, V. O. Bessonov, and A. A. Fedyanin, "Optimization of multilayer photonic structures using artificial neural networks to obtain a target optical response," JETP Lett. **114**, 321 (2021).
6. A. A. Popkova and A. A. Fedyanin, "Convolutional neural networks for predicting morphological and nonlinear optical properties of thin films of quasi-two-dimensional materials," JETP Lett. **118**, 502 (2023).
7. E. Kuprikov, A. Kokhanovskiy, K. Serebrennikov, and S. Turitsyn, "Deep reinforcement learning for self-tuning laser source of dissipative solitons," Sci. Rep. **12**, 7185 (2022).
8. G. A. Kolosov, A. S. Shorokhov, and A. A. Fedyanin, "Numerical simulation of a photonic tensor core for the hardware acceleration of the optical matrix–vector multiplication," JETP Lett. **120**, 932 (2024).
9. B. J. Shastri, A. N. Tait, T. Ferreira de Lima, M. A. Nahmias, H. T. Peng, and P. R. Prucnal, "Principles of neuromorphic photonics," in *Unconventional Computing* (Springer, New York, 2018), p. 83.
10. T. Ferreira De Lima, B. J. Shastri, A. N. Tait, M. A. Nahmias, and P. R. Prucnal, "Progress in neuromorphic photonics," Nanophotonics **6**, 577 (2017).
11. T. J. Naughton and D. Woods, "Optical computing," in *Unconventional Computing* (Springer, New York, 2018), p. 57.
12. A. I. Musorin, A. S. Shorokhov, A. A. Chezhegov, T. G. Baluian, K. R. Safronov, A. V. Chetvertukhin, A. A. Grunin, and A. A. Fedyanin, "Photonics approaches to the implementation of neuromorphic computing," Phys. Usp. **66**, 1211 (2023).
13. H. J. Caulfield, J. Kinser, and S. K. Rogers, "Optical neural networks," Proc. IEEE **77**, 1573 (2002).
14. C. Huang, V. J. Sorger, M. Miscuglio, et al., "Prospects and applications of photonic neural networks," Adv. Phys.: X **7**, 1981155 (2022).
15. X. Lin, Y. Rivenson, N. T. Yardimci, M. Veli, Y. Luo, M. Jarrahi, and A. Ozcan, "All-optical machine learning using diffractive deep neural networks," Science (Washington, DC, U. S.) **361**, 1004 (2018).
16. H. Chen, S. Lou, Q. Wang, P. Huang, H. Duan, and Y. Hu, "Diffractive deep neural networks: Theories, optimization, and applications," Appl. Phys. Rev. **11**, 021332 (2024).
17. Z. Li, F. Liu, W. Yang, S. Peng, and J. Zhou, "A survey of convolutional neural networks: Analysis, applications, and prospects," IEEE Trans. Neural Netw. Learn. Syst. **33**, 6999 (2021).
18. H. Dou, Y. Deng, T. Yan, H. Wu, X. Lin, and Q. Dai, "Residual D^2NN: Training diffractive deep neural networks via learnable light shortcuts," Opt. Lett. **45**, 26882691 (2020).
19. M. Miscuglio, Z. Hu, S. Li, J. K. George, R. Capanna, H. Dalir, P. M. Bardet, P. Gupta, and V. J. Sorger, "Massively parallel amplitude-only Fourier neural network," Optica **7**, 1812 (2020).
20. T. Fujita, H. Sakaguchi, J. Zhang, H. Nonaka, S. Sumi, H. Awano, and T. Ishibashi, "Magneto-optical diffractive deep neural network," Opt. Express **30**, 36889 (2022).
21. Z. Duan, H. Chen, and X. Lin, "Optical multi-task learning using multi-wavelength diffractive deep neural networks," Nanophotonics **12**, 893 (2023).
22. T. Zhou, L. Fang, T. Yan, J. Wu, Y. Li, J. Fan, H. Wu, X. Lin, and Q. Dai, "In situ optical backpropagation training of diffractive optical neural networks," Photon. Res. **8**, 940 (2020).
23. R. C. Gonzalez and R. E. Woods, *Digital Image Processing* (Pearson Education, New York, 2002).
24. T. Yan, J. Wu, T. Zhou, H. Xie, F. Xu, J. Fan, L. Fang, X. Lin, and Q. Dai, "Fourier-space diffractive deep neural network," Phys. Rev. Lett. **123**, 023901 (2019).
25. J. W. Goodman, *Introduction to Fourier Optics* (Roberts and Company, Englewood, Colorado, 2005).
26. V. V. Yushkov, V. A. Sitnyansky, A. S. Shorokhov, and A. A. Fedyanin, "Analog optical correlation augmented by Mie-resonant metasurfaces," ACS Photon. **11**, 2506 (2024).
27. Y. LeCun, C. Cortes, and C. Burges, *MNIST Handwritten Digit Database* (AT&T Labs., 2010).
28. R. E. Blahut, *Fast Algorithms for Digital Signal Processing* (Addison–Wesley, Boston, 1985).
29. H. Wang, W. Zhang, D. Ladika, et al., "Two-photon polymerization lithography for optics and photonics: Fundamentals, materials, technologies, and applications," Adv. Funct. Mater. **33**, 2214211 (2023).
30. E. Goi, X. Chen, Q. Zhang, B. P. Cumming, S. Schoenhardt, H. Luan, and M. Gu, "Nanoprinted high-neuron-density optical linear perceptrons performing near-infrared inference on a CMOS chip," Light Sci. Appl. **10**, 40 (2021).
31. T. G. Baluian, D. I. Pechkurova, A. V. Konovalova, A. A. Popkova, and A. A. Fedyanin, "Free-space and solid-matrix-media diffraction neural network masks made by two-photon lithography," in *Advanced Laser Processing and Manufacturing VIII,* Proc. SPIE **13234**, 132340A (2024).
32. H. Chen, J. Feng, M. Jiang, Y. Wang, J. Lin, J. Tan, and P. Jin, "Diffractive deep neural networks at visible wavelengths," Engineering **7**, 1483 (2021).
33. D. V. Soshnikov, L. L. Doskolovich, G. A. Motz, E. V. Byzov, E. A. Bezus, D. A. Bykov, and N. L. Kazanskiy, "Designing robust diffractive neural networks with improved transverse shift tolerance," J. Opt. Soc. Am. A **42**, 699 (2025).

Translated by the authors

Publisher's Note. Pleiades Publishing remains neutral with regard to jurisdictional claims in published maps and institutional affiliations.
AI tools may have been used in the translation or editing of this article.